



## Use of near-infrared hyperspectral (NIR-HS) imaging to visualize and model the maturity of long-ripening hard cheeses

Hasitha Priyashantha<sup>a,\*</sup>, Annika Höjer<sup>b</sup>, Karin Hallin Saedén<sup>b</sup>, Åse Lundh<sup>a</sup>, Monika Johansson<sup>a</sup>, Gun Bernes<sup>c</sup>, Paul Geladi<sup>d</sup>, Mårten Hetta<sup>c</sup>

<sup>a</sup> Department of Molecular Sciences, Swedish University of Agricultural Sciences, Box 7015, SE-750 07, Uppsala, Sweden

<sup>b</sup> Norrmejerier, Mejerivägen 2, SE-906 22, Umeå, Sweden

<sup>c</sup> Department of Agricultural Research for Northern Sweden, Swedish University of Agricultural Sciences, SE-901 83, Umeå, Sweden

<sup>d</sup> Department of Forest Biomaterials and Technology, Swedish University of Agricultural Sciences, SE-901 83, Umeå, Sweden

### ARTICLE INFO

#### Keywords:

cheese maturation  
Principal component analysis  
Partial least squares regression  
Pixelwise image prediction

### ABSTRACT

Spectroscopic measurements and imaging have great potential in rapid prediction of cheese maturity, replacing existing subjective evaluation techniques. In this study, 209 long-ripening hard cheeses were evaluated using a hyperspectral camera and also sensory evaluated by a tasting panel. A total of 425 NIR hyperspectral (NIR-HS) images were obtained during ripening at 14, 16, 18, and 20 months, until final sensorial approval of the cheese. The spectral data were interpreted as possible compositional changes between scanning occasions. Regression modelling by partial least squares (PLS) was used to explain the relationship between average spectra and cheese maturity. The PLS model was evaluated with whole cheeses (average spectrum), but also pixelwise, producing prediction images. Analysis of the images showed an increasing homogeneity of the cheese over the time of storage and ripening. It also suggested that maturation begins at the center and spreads to the outer periphery of the cheese.

### 1. Introduction

Long-ripening cheeses are important premium products for the dairy sector (Ardö, 1993), but cheese maturation is a costly and not fully controllable or predictable process (Fox et al., 1996). During maturation, the curd turns into a characteristic cheese with a particular flavour and texture depending on the microflora, milk quality, industrial processing steps, and storage conditions (e.g., Fox et al., 1996; Robinson and Wilbey, 1998; Rehn et al., 2010). The characteristic flavour and texture of different long-ripening cheeses are associated with the end-products of lipolysis and proteolysis in the matured cheese (Molina et al., 1999; Collins et al., 2003; Verdini and Rubiolo, 2002).

At present, maturation of long-ripening cheeses is mainly monitored by conventional methods based on chemical characterization and subjective evaluation of organoleptic properties (O'Shea et al., 1996; Coker et al., 2005). Destructive sensory evaluation at regular intervals is used to determine ripeness and readiness for the market. This approach is time-consuming and wastes material, and is therefore expensive for the producer. Thus, rapid non-destructive technologies for monitoring the maturation process in long-ripening cheeses are required. There is great interest in using non-destructive spectroscopic techniques to monitor

cheese maturation and quality (Mazerolles et al., 2001; Downey et al., 2005; Currò et al., 2017; Lei and Sun, 2019). Cheese ripening has been studied with various novel techniques, including ultrasound (Benedito et al., 2001), X-ray computed tomography (Huc et al., 2014), confocal microscopic imaging (Soodam et al., 2014), and magnetic resonance imaging (Huc et al., 2014). During the past decade, near-infrared hyperspectral (NIR-HS) imaging applications have been developed for use as non-destructive quality and safety inspection tools in the food industry (Gowen, O'Donnell, Cullen, Downey and Frias, 2007; Liu et al., 2014). It has been shown that it is possible to use NIR-HS imaging to monitor the ripening of semi-hard cheese packed in transparent vacuum packages (Darnay et al., 2017).

A NIR-HS image is a parallelepiped, three-dimensional data array, sometimes called a hypercube. Two of the dimensions are pixel indices and the third dimension is a wavelength index. Each pixel in the hypercube is a complete spectrum, e.g. 256 wavelength bands from 900 to 2500 nm (Gowen et al., 2007). Identifying the key wavelengths with multivariate methods can improve the predictive capability and accuracy of a model (Burger and Gowen, 2011). Pre-processing of the images to improve the spectral information and to prepare data for further processing is therefore an important step in model development

\* Corresponding author.

E-mail address: [hasi.tvp@slu.se](mailto:hasi.tvp@slu.se) (H. Priyashantha).

(Gowen et al., 2007). Due to the nature of the technique, both qualitative and quantitative analyses are possible with NIR-HS imaging, using spectroscopic and multivariate calibration techniques (Burger and Geladi, 2005). Advances in the hyperspectral imaging technique, integrating NIR imaging and spectroscopy, provide novel possibilities to analyse and characterize the spatial and spectral information on the sample of interest (Gowen et al., 2007). Each pixel in the NIR-HS image provides information based on the spectrum of that unique position, and thus allows visualization of the biochemical constituents and their distribution in the sample.

The objective of this study was to develop and evaluate predictive models based on the NIR-HS imaging technique for monitoring ripening of long-ripening cheeses. The hypothesis tested was that NIR-HS imaging, coupled with chemometric techniques, can predict the maturity and ripening process in paraffin wax-covered long-ripening hard cheeses in a commercial cheese manufacturing setting.

## 2. Material and methods

### 2.1. Cheese material and experimental design

This study was conducted in a full-scale commercial cheese manufacturing process at Norrmejerier, Sweden and was part of a larger project, in which raw milk used for cheese production was sampled and characterized twice a month during one year. The cheese resulting from the analyzed milk was subsequently used for this study. During the study, 209 cheeses were scanned (NIR-HS imaging) from February 2016 to February 2017, resulting in a set of 425 NIR-HS images. Each cheese comprised an 18 kg cylinder (40 cm diameter, 14 cm height) that was brine-salted to a content of around 1.2% NaCl, coated with paraffin wax, and ripened for at least 14 months under conditions previously described by Rehn et al. (2010). After 14 months of ripening, the cheeses were evaluated for maturity and organoleptic quality by a sensory panel, and this was repeated every two months until 20 months after production. At least three trained sensory panellists from the dairy company evaluated each cheese against a standard protocol considering outer appearance, flavour, smell and texture. Thereby, the three sensory panellists collectively determined whether the cheese could be considered sensorially approved (mature) or not. When a cheese was considered sufficiently mature, it was removed from the study and sent to the market for sale. If a cheese was considered to be still immature, it was sent back to the cheese-ripening facility and re-evaluated after another two months of storage. The NIR-HS images were captured in parallel with the sensorial evaluation of the cheeses, irrespective of the sensory approval. As a consequence of the analytical procedure, faster-maturing cheeses were sampled, evaluated by the sensory panel, and scanned by the NIR-HS camera on fewer occasions than slower-maturing cheeses. Not all cheeses were studied at every scanning occasion, and therefore different numbers of NIR-HS images were produced at each scanning occasion. The procedure resulted in 425 images obtained from 209 individual cheeses varying in age and maturity (Fig. 1). Out of these 425 HS images, 81 were acquired from sensorially approved cheeses that at this point exited the study, while 344 images were obtained from cheeses that were not yet approved. The chronological age (days) of each cheese was calculated as the difference between production date and imaging date.

### 2.2. Hyperspectral imaging system

To acquire NIR-HS images, an Umbio Inspector (Umbio AB, Umeå, Sweden) line-scan pushbroom system equipped with a moving belt was used as described in the literature (Geladi et al., 2007). The HS imaging system was set up as described by Hetta et al. (2017). In brief, a line-scan pushbroom system was used with a line-scan camera with a 22.5 mm sisuChema SWIR (short-wave infrared) objective (Specim, Spectral Imaging Ltd., Oulu, Finland) and equipped with a HgCdTe 2-D

array detector. The spectral range recorded was 937–2542 nm at increments of 6 nm, resulting in a NIR-HS image (variable length x 320 pixels width) in 256 wavelength channels. Scanning speed was set to acquire square pixels.

### 2.3. Hyperspectral image acquisition

The cheeses were covered with a 1-mm layer of paraffin wax. They were carefully placed on the conveyor belt on the defined scanning occasions (14, 16, 18, and 20 months) to acquire the NIR-HS images. The cheeses were, however, not oriented in exactly the same way on the different scanning occasions. Illumination was supplied by quartz-halogen lamps at a 45-degree angle as a radiation source. For dark and white references, a shutter and a white spectralon surface, respectively, were used, and pseudo-absorbance was calculated. Reflectance standards are essential for image calibration, to correct pixel-to-pixel variations arising due to inconsistencies in capture and illumination of samples (Burger and Geladi, 2005). Each image had approximately 350 000 pixels, of which approximately 63% were cheese pixels and 37% represented background pixels. The average spectra of the images (cheese pixels) were calculated and modelled using Breeze and Evince software (Prediktera AB, Umeå, Sweden). The key steps in the imaging and data analysis procedure are illustrated in Fig. 2.

### 2.4. Image transformation and cleaning

Reflectance images ( $I_{\text{raw}}$ ) were recorded using the dark ( $I_{\text{dark}}$ ) and white ( $I_{\text{white}}$ ) reference data and the reflectance was transformed into absorbance ( $A$ ) using the equation:  $A = -\log_{10} [(I_{\text{raw}} - I_{\text{dark}}) / (I_{\text{white}} - I_{\text{dark}})]$ , according to Grahn et al. (2016). NIR-HS imaging captures a square-shaped image and the area surrounding the circular cheese was thus background information, giving rise to a noisy spectrum that needed to be eliminated before further processing. The background information (pixels representing the bare belt) was eliminated by removing absorbances over 1.5 at band 55 (1279 nm), to provide the best possible difference between the sample and the background. Objects in the images smaller than 1000 square pixels in total area were also removed.

### 2.5. Hyperspectral image analysis

The NIR-HS image analysis was conducted using the Evince software. In section 3.1, analysis of a single cheese is described in order to illustrate the analytical method. In section 3.2, the analytical method is also demonstrated using an individual cheese at four maturity levels, forming a composite image. The tools in the Evince software were used to create informative diagrams explaining the spectral and maturity differences in the cheeses.

### 2.6. Partial least squares discriminant analysis

Because the maturity criteria were only available for whole cheeses, the cheese NIR-HS images were replaced by average spectra after background removal. Noisy wavelengths were further removed by excluding wavelengths below 1000 nm and above 2400 nm. The spectra were used in the standard normal variate (SNV)-corrected and mean-centered form. A partial least squares (PLS) discriminant model was applied to a training dataset ( $n = 100$  NIR-HS images). The maturity of the cheeses, expressed in days, was used to make the PLS calibration models. The diagnostics used for the selected PLS model were coefficient of determination for calibration ( $R^2$ ) and root mean squared error of calibration (RMSEC).

### 2.7. Image visualization and distribution map

The maturity attributes for all pixels were predicted using the

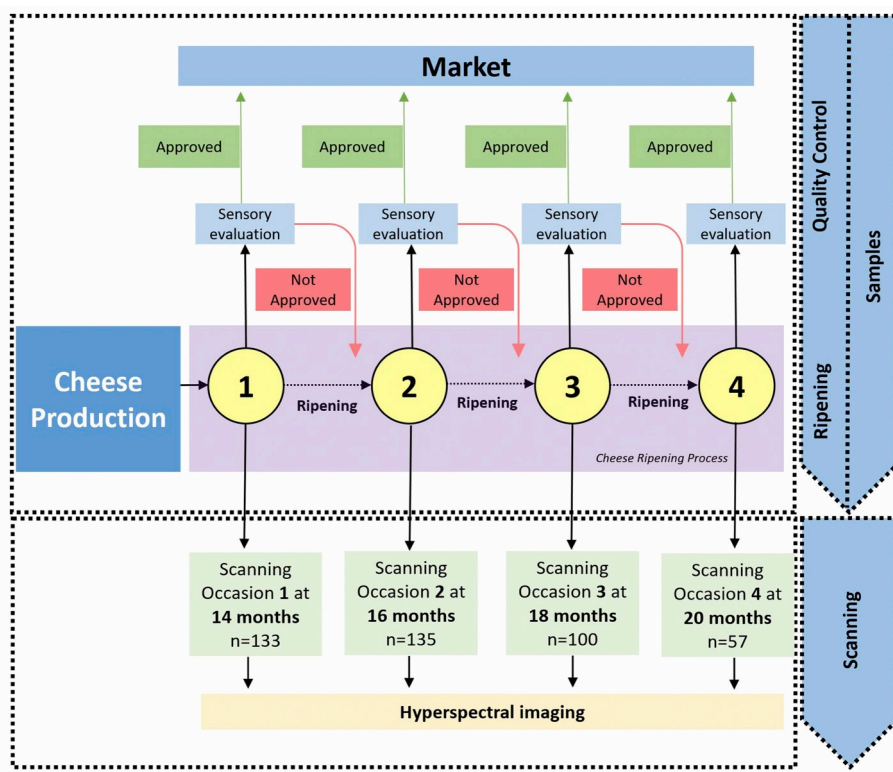


Fig. 1. Flow chart of sample handling and study design. Note: Not all cheeses remained throughout the study and, for practical reasons, not all cheeses were scanned on every occasion. This resulted in different numbers (n) of NIR-hyperspectral images on each scanning occasion.

calibration model developed from the training dataset. Predicted maturity values were applied to the region of interest (ROI) in the test dataset and distribution maps were developed for each cheese image. A high level of smoothing by merging  $15 \times 15$  pixels was applied to pixels within the ROI, to improve the clarity of the pixels in the larger image.

### 3. Results and discussion

#### 3.1. Hyperspectral analysis of an individual cheese

In Fig. 3A, a 14-month-old cheese is shown as a principal component one (PC1) image, coloured according to PC1 values (in the order

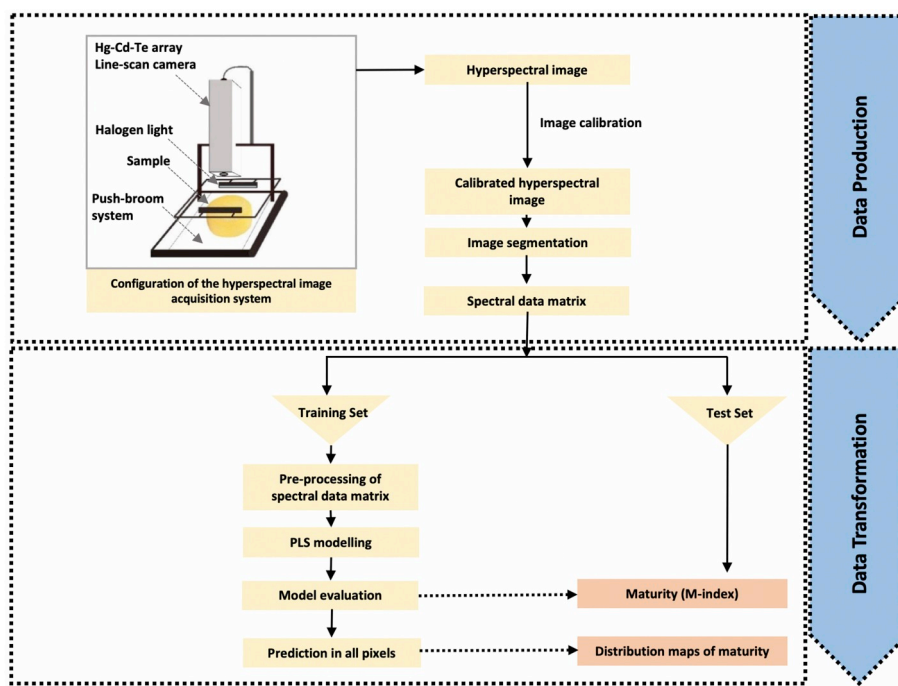


Fig. 2. Flow chart of the hyperspectral imaging, pre-processing, and partial linear squares (PLS) modelling procedure used for quantifying and predicting the maturity of long-ripening hard cheeses.

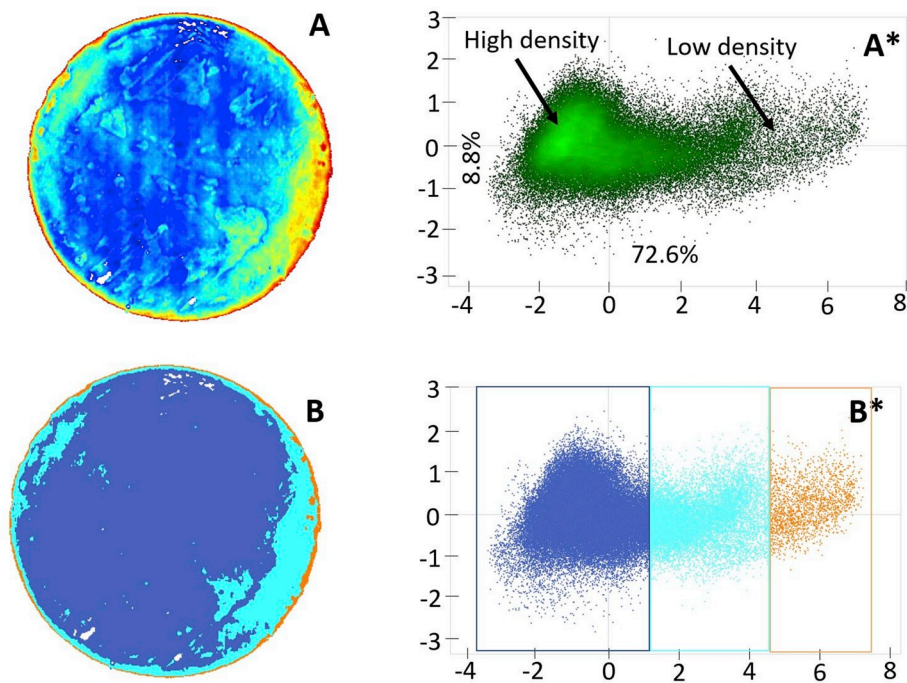


Fig. 3. A) The first principal component (PC1) of a 14-month-old cheese, colour-coded by PC1 values. A\*) PC1 vs. PC2 score scatter plot of pixels of the same cheese, indicating different pixel intensity areas in PC1. B\*) Preliminary selection of class regions (rectangular) in the score plot. B) Image coloured according to the classes selected in B\* and projected onto the whole cheese using identical colours. The diagram should be read in the order A→A\*→B\*→B. (For interpretation of the references to colour in this figure legend, the reader is referred to the Web version of this article.)

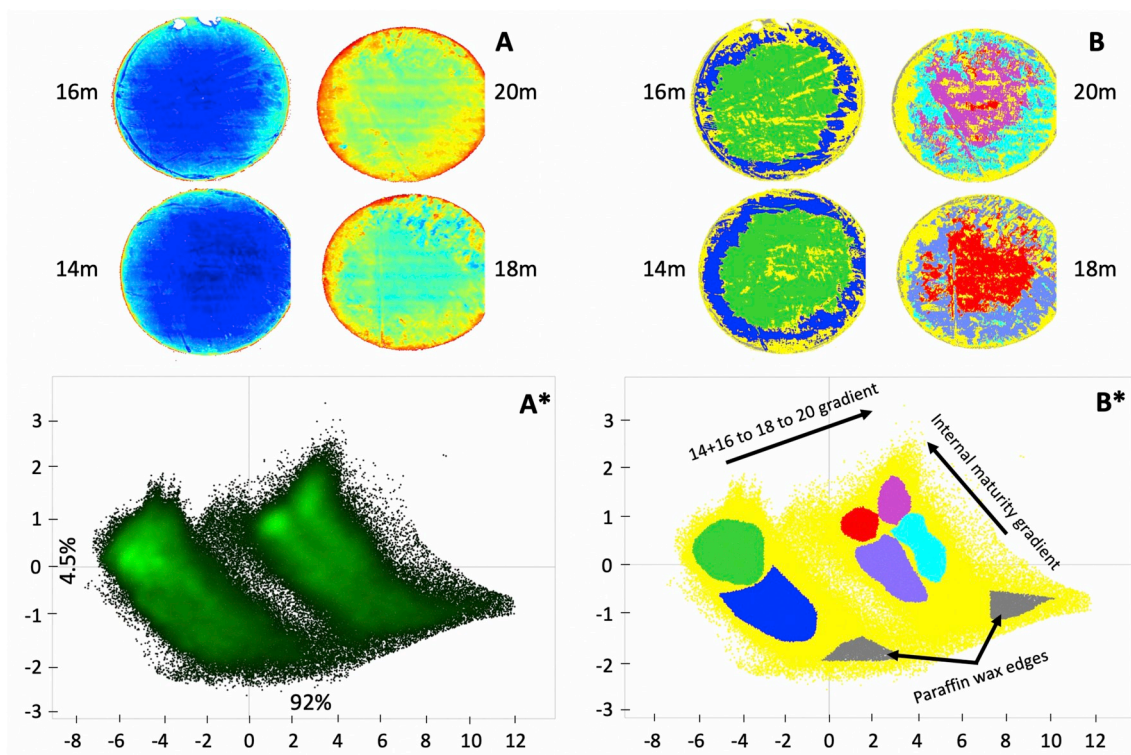
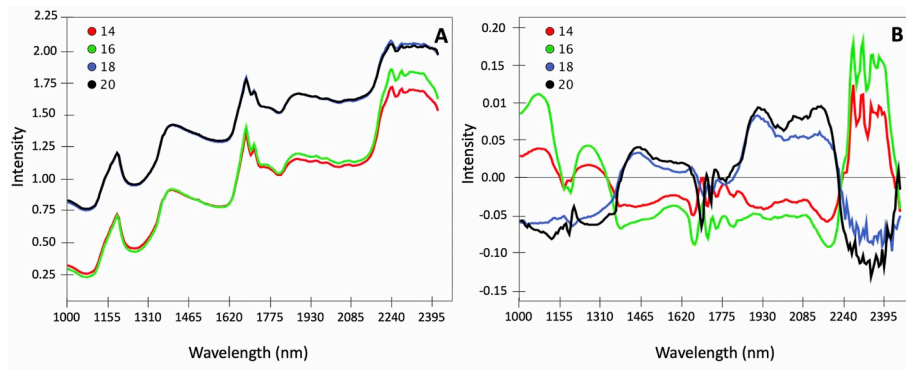


Fig. 4. A) Composite of the cheese at different maturity stages (14, 16, 18, 20 months), showing the first principal component (PC1) score. A\*) PC1 vs. PC2 score scatter plot for the composite image in A. B\*) Manually selected regions of interest in the score scatter plot in A\*. B) Projection of the regions selected in B\* on the composite image. Colour codings are identical for B and B\*. The diagram should be read in the order A→A\*→B\*→B. (For interpretation of the references to colour in this figure legend, the reader is referred to the Web version of this article.)

blue (lowest), cyan, green, yellow, orange, red (highest)). In order to interpret these images, a score scatter plot was created, as shown in Fig. 3A\*. Three major regions with different score values and different densities, obtained after making a preliminary selection of three rectangular ROI (classes), are shown as coloured regions along PC1 in Fig. 3B\*. The classes can also be seen in the coloured score image in Fig. 3B, produced using identical colours as in Fig. 3B\*.

Different regions in the cheese were revealed, with the edge of the cheese (red, yellow) mainly consisting of paraffin wax. Inside the cheese, two main regions were observed based on pixel intensities and PC1 (cyan and blue, respectively).



**Fig. 5.** A) Non-transformed and b) standard normal variate (SNV)-transformed spectral data for one randomly selected cheese scanned at 14, 16, 18, and 20 months after production.

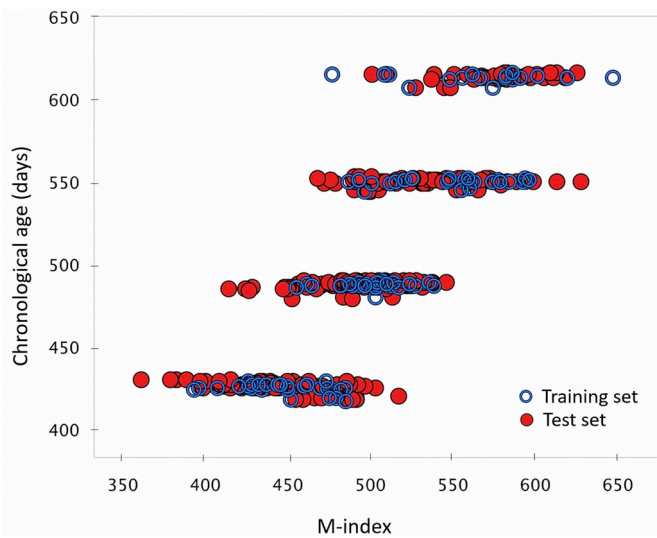


**Fig. 6.** Performance of the best prediction partial least squares (PLS) model for quantifying cheese maturity. Chronological age of the cheeses (423, 487, 550, and 614 days, corresponding to 14, 16, 18 and 20 months, respectively) was taken as the difference (days) between production data and imaging date. M-index: maturity index developed using NIR-hyperspectral image analysis.

**3.2. Hyperspectral analysis of a composite image of a cheese at four maturity levels**

The procedure described in section 3.1 for one cheese was repeated for the same cheese at different ages (14, 16, 18, and 20 months). The four images were made into a composite (Fig. 4A). After PCA and mean-centering of the composite image, a score scatter plot was obtained

(Fig. 4A\*). It revealed two large pixel clusters, one with a sub-set of pixels consisting of two separable clusters, forming three different main pixel clusters, i.e., 14 and 16 months maturity together and a sub-set of 18 and 20 months maturity levels (Fig. 4A\*). In one of the large clusters, there was a region of high pixel density and a gradient away from it, i.e., a combined high pixel density area for the cluster of the cheese at 14 and 16-months of age. In the other large cluster, there were two high pixel density areas and their gradients within the sub-set of the cheese at 18 and 20-months of age. Pixel clusters and intensity gradients may relate to the maturity of the cheese. The three major high pixel density areas observed in Fig. 4A\* were manually selected as shown in Fig. 4B\* (green, red, and magenta). There were also gradients connected to each of the three clusters in Fig. 4A\* and these were manually selected as shown in Fig. 4B\* (blue, purple, and cyan). The selected regions of Fig. 4B\* are shown in Fig. 4B using identical colours. Furthermore, some small clusters were identified in Fig. 4A\* and coloured grey (Fig. 4B\*). The smaller cluster in the lower part of Fig. 4A\* turned out to represent the paraffin wax cover on the cheese. The yellow colour represents uncategorized pixels (Fig. 4B). The changes in colour illustrated in Fig. 4 indicates the occurrence of chemical changes, observed as spectral changes, that relate to age in months, and differences and gradients in composition within the cheese. A detailed discussion of possible explanations for this variation in composition is provided in section 3.3.

**3.3. Wavelengths and their transformations**

It is not meaningful to show many spectra at the same time, since the image becomes confusing. We therefore selected a single cheese for which spectra associated with the different months were representative for the whole dataset. For reasons of clarity, only the four average spectra (14, 16, 18, and 20 months) for this individual cheese presented

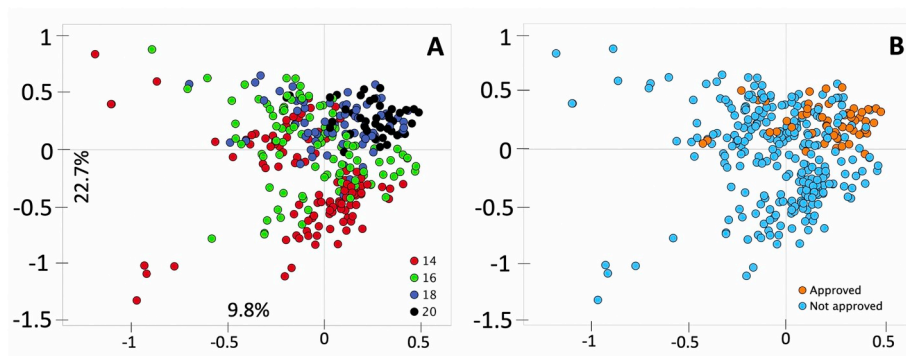


**Fig. 7.** A) Partial least squares (PLS) score scatter plot (component 2 vs. 3) of cheeses imaged at 14, 16, 18, and 20 months after production. B) PLS score scatter plot of the values in plot A, coloured according to approved or not approved for market by the sensory panel.

**Table 1**

Comparison of age and predicted maturity index (M-index), both in days, for six cheeses scanned at 14, 16, 18, and 20 months after production.

Cheese ID	1st scan, 14 months			2nd scan, 16 months			3rd scan, 18 months			4th scan, 20 months		
	Age	M-index	Dif									
C1	419	436	17	488	473	-15	551	538	-13	614	594	-20
C2	419	445	26	488	483	-5	551	554	3	614	613	-1
C3	419	466	47	488	498	10	551	580	29	614	626	12
C4	418	454	36	487	488	1	550	557	7	613	612	-1
C5	425	473	48	487	529	42	550	534	-16	613	571	-42
C6	425	477	52	487	532	45	550	568	18	613	597	-16

Calculations performed using the PLS model as described in section 3.5. Dif = difference between M-index and age of the cheese in days.

in Fig. 4 is shown in Fig. 5. Higher absorbance intensities were observed for the cheese scanned at 18 and 20 months compared with the same cheese scanned at 14 and 16 months (Fig. 5A). The reasons for this could be higher density (Darnay et al., 2017) and loss of gases and water during ripening (Hickey et al., 2013).

As shown in Fig. 5B, there were differences between the cheese at younger (14 and 16 months) and older (18 and 20 months) age in terms of SNV-corrected absorbance intensity at a given wavelength. These differences reflect the chemical changes that occur as a function of ripening. To relate the chemical components responsible for the differences in spectra, we compared the results against typical wavelengths reported for milk by Šašić and Ozaki (2000), who assigned differences observed in the 1208 nm band to milk fat (CH, CH<sub>2</sub>, and CH<sub>3</sub> bonds). According to Fig. 5B, the intensity in this band was higher for the cheese at 14 and 16 months than for the same cheese at 18 and 20 months of age. Due to lipolysis of fat during ripening, less intact milk fat is available in older cheeses compared with young cheeses (McSweeney, 2004). Šašić and Ozaki (2000) assigned band 2056 and 2160 nm to amides. In our case, the intensities in the 2056 and 2160 bands were higher in the more mature cheese than in the younger cheese, indicating build-up of amides during ripening (McSweeney, 2004). The bands at 2316, 2340, and 2368 nm arise from combinations of CH<sub>2</sub> stretching and bending modes of protein side-chain groups (Šašić and Ozaki, 2000). In the present case, the intensities were higher for the younger compared with the older cheese, probably due to higher protein content (McSweeney, 2004). Our observations support findings by Hickey et al. (2013) that proteolysis increases during ripening.

### 3.4. PLS model between average spectra and age

The hyperspectral analyses (Figs. 3 and 4) reveal much about the cheese and variations in its maturity. The effect of chronological aging and changes due to maturity and differences between internal regions of the cheese are apparent. However, presenting corresponding data for hundreds of cheeses in a similar way would be tedious and nearly impossible to handle. Fortunately, it was found that the average spectra (Fig. 5) could also be used to show differences in ripening. An attempt was therefore made to build a multivariate regression model of average spectra of all the scanned cheeses and their respective age. A PLS model was developed using average spectra calculated from the images for each cheese and their corresponding age in days. The dataset was split into a training set (n = 100 NIR-HS images) and a test set (n = 325 NIR-HS images), with the same distribution of scanning occasions.

The performance of the best PLS prediction model in assessing the maturity of the cheeses is shown in Fig. 6. The performance of the model was evaluated using the R<sup>2</sup> and RMSEC values; the higher the R<sup>2</sup> value and the lower the RMSEC value, the more powerful the model as a prediction tool (Vigneau et al., 2011). Five PLS components were found to be sufficient for the model. For the proposed model, R<sup>2</sup> was 0.76 and RMSEC was 36 days of age. The model was calibrated using cross-validation, resulting in root mean square error for the cross-validation of 34 days. The validated model was then used with the test set

and its performance was evaluated with root mean square error for prediction, which was found to be 36 days.

The maturity (M) index and cheese age show a linear relationship until 18 months (~550 days), at which point a shift is observed. This indicates that cheeses older than 18 months needed a longer time to reach maturity and seem to follow a different pattern. There is a large variation in M-index for the cheeses on each particular scanning occasion (chronological age) (Fig. 6).

### 3.5. Scores of the PLS model

By using partial least squares regression (PLSR), quantitative estimates of particular relationships between the target variables and the spectral response were obtained. These were used to predict the concentration of different components in each pixel and to visualize their spatial distribution in the sample (see Vigneau et al., 2011). The PLS score scatter plot of components 2 and 3, describing the most meaningful variation in cheese maturity, showed that there was more variation between cheeses on the earlier scanning occasions (younger cheeses) than on the later scanning occasions (older cheeses), when they clustered together (Fig. 7A). Component 1 was not important and is possibly influenced by the paraffin wax layer, and was therefore not considered. This is in agreement with the diagram showing the same score scatter plot, but coloured in relation to approval by the sensory panel (Fig. 7B). To be approved by the sensory panel, a cheese has to have achieved certain characteristic properties and most of the approved cheeses were likely to be among the older ones. However, this could be partly due to the design of the study, as older approved cheeses were not scanned further and instead sent to market. The variation was greatest among the cheeses that were not approved by the panel and is likely to derive from the young cheeses scanned on the earlier scanning occasions. Cheeses that were approved for the market, most of them originating from the scanning occasions at 18 and 20 months after production, showed less variation in the PLS score scatter plot (Fig. 7).

Table 1 shows the predicted maturity and the actual age for a selected set of six cheeses (C1-C6). On the earlier scanning occasions, the predicted maturity, i.e., M-index, tended to be higher than the age of the cheese. In contrast, towards the end of ripening, i.e., on the later scanning occasions, the predicted M-index mostly tended to be lower than the actual age of the cheese. This observation supports what was mentioned previously; that the more slowly maturing cheeses are kept in the cycle and faster maturing cheeses leave the study for the market.

### 3.6. Image visualization and distribution map

The PLS regression model for prediction of cheese maturity was applied to hypercubes of selected cheese images from different scanning occasions to visualize the maturity distribution of individual cheeses. A high level of image smoothing was applied to obtain visually comparable maturity distribution maps (non or intermediate levels of smoothing were found to give noisy results in our preliminary studies).

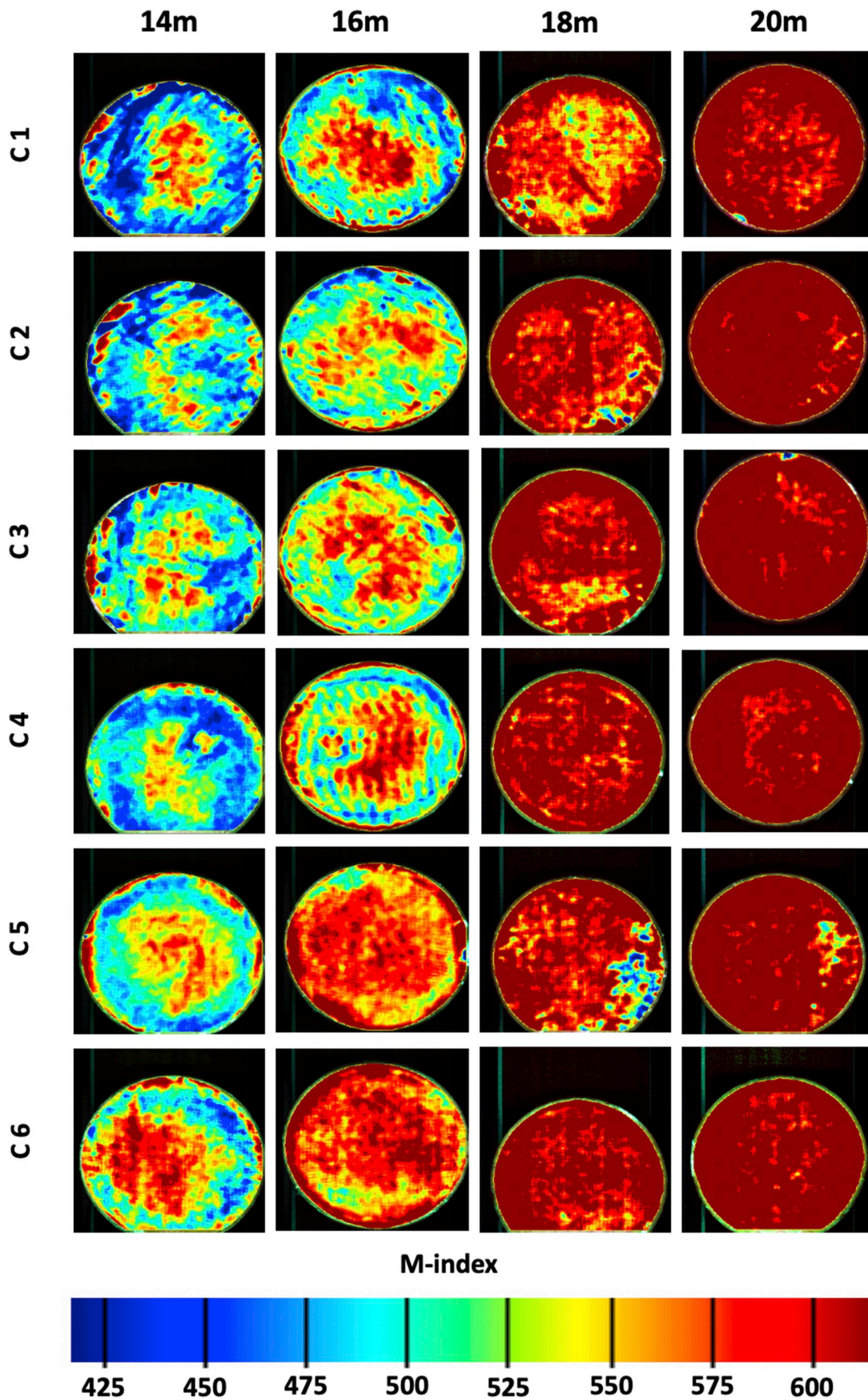


Fig. 8. Spatial distribution of maturity (M-) index in cheeses C1-C6 (see Table 1) on four different scanning occasions (14, 16, 18, and 20 months, corresponding to 423, 487, 550, and 614 days of age). M-index was developed using the PLS model, as described in section 3.4.

Fig. 8 shows the distribution of maturity in the six selected cheeses (C1–C6 in Table 1) on the four scanning occasions.

The images in Fig. 8 suggest that cheese maturation is non-homogeneous, i.e., within each cheese some parts are more mature than others. Moreover, the images indicate that ripening starts from the center of the cheese and moves to the outer periphery of the cheese rind. Similarly, as found in the PCA analysis (Fig. 4B), the images reveal that there are variations within an individual cheese and also within maturity level. For the 14- and 16-month cheeses in Fig. 8, green indicates the more mature center and blue the less mature edge. For the 18-month cheeses, red indicates the more mature center and purple the less mature edge. For the 20-month cheeses, the more mature center is coloured as magenta and the less mature edge is cyan.

Cheeses scanned on a particular occasion after production may have reached different degrees of maturity, thus showing different distributions of ripening of the curd (Fig. 8). This indicates that cheeses ripen internally in an uneven way and that variation occurs both within and between cheeses.

#### 4. Conclusions

NIR-HS imaging is a powerful non-destructive method that provides the advantage of exploring simultaneous spatialized spectral information in each pixel. In the present study, NIR-HS imaging made it possible to generate meaningful composition classes based on individual images of a cheese and on a composite image representing a cheese at four maturity levels. Using chemometric and exploratory visualization techniques, the data were processed into meaningful and comprehensible information. The NIR-HS images provide indications on the chemical composition and on changes taking place during cheese ripening, potentially allowing prediction of cheese maturity. Considering that the model developed in our study achieved 76% accuracy in prediction of maturity (M-index), we conclude that the technique can become an important tool in cheese production for optimizing logistics and ensuring efficient use of costly cheese-ripening facilities.

#### Declaration of interest form

None.

#### Ethical statement

#### Conflicts of interest

The authors declare no conflicts of interest.

#### Ethical approval

This article does not contain any studies with human participants or animals performed by any of the authors.

#### Informed consent

Written informed consent was obtained from all study participants.

#### Acknowledgments

This study was conducted with the financial support from The Swedish Farmers' Foundation for Agricultural Research (grant number O-16-20-764), The Regional Farmers Foundation for Agricultural Research in Northern Sweden and the Kamprad Family Foundation (grant number 20160098), which are gratefully acknowledged for research grants. Special thanks to Andreas Vidman and Oskar Jonsson at Prediktera AB for assistance with the software.

#### References

- Ardö, Y., 1993. Swedish cheese varieties. In: 2nd ed. In: Fox, P.F. (Ed.), *Cheese: Chemistry, Physics And Microbiology*, vol. 2. Chapman and Hall, London, UK, pp. 254–256.
- Benedito, J., Carcel, J., Gisbert, M., Mulet, A., 2001. Quality control of cheese maturation and defects using ultrasonics. *J. Food Sci.* 66 (1), 100–104. <https://doi.org/10.1111/j.1365-2621.2001.tb15589.x>.
- Burger, J., Geladi, P., 2005. Hyperspectral NIR image regression part I: calibration and correction. *J. Chemom.* 19 (5–7), 355–363. <https://doi.org/10.1002/cem.938>.
- Burger, J., Gowen, A., 2011. Data handling in hyperspectral image analysis. *Chemometr. Intell. Lab. Syst.* 108 (1), 13–22. <https://doi.org/10.1016/j.chemolab.2011.04.001>.
- Coker, C.J., Crawford, R.A., Johnston, K.A., Singh, H., Creamer, L.K., 2005. Towards the classification of cheese variety and maturity on the basis of statistical analysis of proteolysis data—a review. *Int. Dairy J.* 15 (6), 631–643. <https://doi.org/10.1016/j.idairyj.2004.10.011>.
- Collins, Y.F., McSweeney, P.L.H., Wilkinson, M.G., 2003. Lipolysis and free fatty acid catabolism in cheese: a review of current knowledge. *Int. Dairy J.* 13 (11), 841–866. [https://doi.org/10.1016/S0958-6946\(03\)00109-2](https://doi.org/10.1016/S0958-6946(03)00109-2).
- Curro, S., Manuelian, C.L., Penasa, M., Cassandro, M., De Marchi, M., 2017. Technical note: feasibility of near infrared transmittance spectroscopy to predict cheese ripeness. *J. Dairy Sci.* 100 (11), 8759–8763. <https://doi.org/10.3168/jds.2017-13001>.
- Darnay, L., Králik, F., Oros, G., Koncz, Á., Firtha, F., 2017. Monitoring the effect of transglutaminase in semi-hard cheese during ripening by hyperspectral imaging. *J. Food Eng.* 196, 123–129. <https://doi.org/10.1016/j.jfoodeng.2016.10.020>.
- Downey, G., Sheehan, E., Delahunty, C., O'Callaghan, D., Guinee, T., Howard, V., 2005. Prediction of maturity and sensory attributes of Cheddar cheese using near-infrared spectroscopy. *Int. Dairy J.* 15 (6), 701–709. <https://doi.org/10.1016/j.idairyj.2004.06.013>.
- Fox, P.F., Wallace, J.M., Morgan, S., Lynch, C.M., Niland, E.J., Tobin, J., 1996. Acceleration of cheese ripening. *Antonie Leeuwenhoek* 70 (2–4), 271–297. <https://doi.org/10.1007/BF00395937>.
- Geladi, P.L.M., Grahn, H.F., Burger, J.E., 2007. Multivariate images, hyperspectral imaging: background and equipment. In: *Techniques and Applications of Hyperspectral Image Analysis*, pp. 1–15. <https://doi.org/10.1002/9780470010884.ch1>.
- Gowen, A.A., O'Donnell, C.P., Cullen, P.J., Downey, G., Frias, J.M., 2007. Hyperspectral imaging – an emerging process analytical tool for food quality and safety control. *Trends Food Sci. Technol.* 18 (12), 590–598. <https://doi.org/10.1016/j.tifs.2007.06.001>.
- Grahn, H., Geladi, P., Esbensen, K., 2016. *Multivariate and hyperspectral image analysis*. In: Meyers, Robert (Ed.), *Encyclopedia of Analytical Chemistry*. Wiley, New York.
- Hetta, M., Mussadiq, Z., Wallsten, J., Halling, M., Swensson, C., Geladi, P., 2017. Prediction of nutritive values, morphology and agronomic characteristics in forage maize using two applications of NIRS spectrometry. *Acta Agric. Scand. Sect. B Soil Plant Sci* 67 (4), 326–333. <https://doi.org/10.1080/09064710.2017.1278782>.
- Hickey, D.K., Guinee, T.P., Hou, J., Wilkinson, M.G., 2013. Effects of variation in cheese composition and maturation on water activity in Cheddar cheese during ripening. *Int. Dairy J.* 30 (1), 53–58. <https://doi.org/10.1016/j.idairyj.2012.11.006>.
- Huc, D., Challos, S., Monziols, M., Michon, C., Mariette, F., 2014a. Spatial characterisation of eye-growing kinetics in semi-hard cheeses with propionic acid fermentation. *Int. Dairy J.* 39 (2), 259–269. <https://doi.org/10.1016/j.idairyj.2014.06.010>.
- Huc, D., Roland, N., Grenier, D., Challos, S., Michon, C., Mariette, F., 2014b. Influence of salt content on eye growth in semi-hard cheeses studied using magnetic resonance imaging and CO<sub>2</sub> production measurements. *Int. Dairy J.* 35 (2), 157–165. <https://doi.org/10.1016/j.idairyj.2013.11.010>.
- Lei, T., Sun, D.-W., 2019. Developments of nondestructive techniques for evaluating quality attributes of cheeses: a review. *Trends Food Sci. Technol.* 88, 527–542. <https://doi.org/10.1016/j.tifs.2019.04.013>.
- Liu, D., Sun, D.-W., Zeng, X.-A., 2014. Recent advances in wavelength selection techniques for hyperspectral image processing in the food industry. *Food Bioprocess Technol.* 7 (2), 307–323. <https://doi.org/10.1007/s11947-013-1193-6>.
- Mazerolles, G., Devaux, M.-F., Duboz, G., Duployer, M.-H., Riou, N., Dufour, É., 2001. Infrared and fluorescence spectroscopy for monitoring protein structure and interaction changes during cheese ripening. *Lait* 81 (4), 509–527. <https://doi.org/10.1051/lait:2001148>.
- McSweeney, P.L.H., 2004. Biochemistry of cheese ripening: introduction and overview. In: Fox, Patrick F., McSweeney, P.L.H., Cogan, T.M., Guinee, T.P. (Eds.), *Cheese: Chemistry, Physics and Microbiology*, pp. 347–360. [https://doi.org/10.1016/S1874-558X\(04\)80073-3](https://doi.org/10.1016/S1874-558X(04)80073-3).
- Molina, E., Ramos, M., Alonso, L., López-Fandiño, R., 1999. Contribution of low molecular weight water soluble compounds to the taste of cheeses made of cows', ewes' and goats' milk. *Int. Dairy J.* 9 (9), 613–621. [https://doi.org/10.1016/S0958-6946\(99\)00131-4](https://doi.org/10.1016/S0958-6946(99)00131-4).
- O'Shea, B.A., Uniacke-Lowe, T., Fox, P.F., 1996. Objective assessment of cheddar cheese quality. *Int. Dairy J.* 6 (11), 1135–1147. [https://doi.org/10.1016/0958-6946\(95\)00065-8](https://doi.org/10.1016/0958-6946(95)00065-8).
- Rehn, U., Petersen, M.A., Saedén, K.H., Ardö, Y., 2010. Ripening of extra-hard cheese made with mesophilic DL-starter. *Int. Dairy J.* 20 (12), 844–851. <https://doi.org/10.1016/j.idairyj.2010.06.001>.
- Robinson, R.K., Wilbey, R.A., 1998. Cheese maturation. In: *Cheesemaking Practice*, pp. 271–287. [https://doi.org/10.1007/978-1-4615-5819-4\\_15](https://doi.org/10.1007/978-1-4615-5819-4_15).
- Šašić, S., Ozaki, Y., 2000. Band Assignment of near-infrared spectra of milk by use of partial least-squares regression. *Appl. Spectrosc.* 54 (9), 1327–1338. <https://doi.org/10.1366/0003702001951002>.
- Soodam, K., Ong, L., Powell, I.B., Kentish, S.E., Gras, S.L., 2014. The effect of milk protein

- concentration on the microstructure and textural properties of full fat cheddar cheese during ripening. *Food Bioprocess Technol.* 7 (10), 2912–2922. <https://doi.org/10.1007/s11947-014-1342-6>.
- Verdini, R.A., Rubiolo, A.C., 2002. Texture changes during the ripening of port salut argentino cheese in 2 sampling zones. *J. Food Sci.* 67 (5), 1808–1813. <https://doi.org/10.1111/j.1365-2621.2002.tb08727.x>.
- Vigneau, N., Ecartot, M., Rabatel, G., Roumet, P., 2011. Potential of field hyperspectral imaging as a non destructive method to assess leaf nitrogen content in Wheat. *Field Crop. Res.* 122 (1), 25–31. <https://doi.org/10.1016/j.fcr.2011.02.003>.